Robust Active Disturbance Rejection Control of Induction Motor Systems Based on Additional Sliding-Mode Component

Francesco Alonge, *Member, IEEE*, Maurizio Cirrincione, *Senior Member, IEEE*, Filippo D'Ippolito, *Member, IEEE*, Marcello Pucci, *Senior Member, IEEE*, and Antonino Sferlazza, *Member, IEEE*

***Abstract*—This paper deals with motion control systems with induction motor, subject to severe requirements on both dynamics and steady-state behavior. The proposed control methodology could be viewed as an advancement of the standard field oriented control. It consists of two control loops, i.e., the rotor flux and the speed control loops, designed using the active disturbance rejection control method, with the aim to cope with both exogenous and endogenous disturbances, which are estimated by means of two linear extended state observers and then compensated. Moreover, with the aim of achieving total robustness, a sliding-mode based component is designed, in order to take into account disturbance estimation errors and uncertainties in the knowledge of the control gains. The effectiveness of this approach is shown by means of numerical simulations, and experiments carried out on a suitably developed test set-up. Finally, experimental comparisons between the proposed robust active disturbance rejection control, and the basic active disturbance rejection control are given.**

***Index Terms*—Extended state observer (ESO), induction motors (IMs), rejection of disturbances, sliding-mode (SM) control, state feedback.**

Manuscript received February 23, 2016; revised May 13, 2016, September 28, 2016, and December 17, 2016; accepted January 29, 2017. Date of publication March 2, 2017; date of current version June 9, 2017. This work was supported in part by the Italian Ministry of Education, University and Research: Robotic Assisted Driving (RoAD), a research project of national interest (PRIN2012); in part by RITmare, Italian Research for the Sea, under Grant CUP: B91J11000740001; in part by TESEO, High efficiency technologies for on-board energy and environmental sustainability, under Grant CUP: B61C12000850005; and in part by CNR per il Mezzogiorno (Advanced Technologies for Energy Efficiency and Sustainable Mobility) under Grant CUP: B51J10001290001.

F. Alonge, F. D'Ippolito, and A. Sferlazza are with the Department of Energy, Information Engineering and Mathematical Models, University of Palermo, 90128 Palermo, Italy (e-mail: francesco.alonge@unipa.it; filippo.dippolito@unipa.it; antonino.sferlazza@unipa.it).

M. Cirrincione is with the School of Engineering, University of the South Pacific, Suva, Fiji Islands (e-mail: m.cirrincione@ieee.org).

M. Pucci is with the Institute on Intelligent Systems for Automation—Italian National Research Council, 90128 Palermo, Italy (e-mail: pucci@pa.issia.cnr.it).

Color versions of one or more of the figures in this paper are available online at http://ieeexplore.ieee.org.

Digital Object Identifier 10.1109/TIE.2017.2677298

I. Introduction

THIS paper deals with high-performance robust controllers for motion control systems with induction motors (IMs). Many standard controllers have been widely described in the literature employing FOC methodology such as PID-type linear controllers based on the cascade control method, in which four control loops are designed independently of one another aimed to force the rotor flux, speed, direct and quadrature current components to track their references [1]. The control theory, however, offers an important corpus of nonlinear control methodologies for dealing with highly nonlinear systems. Among these, one is the so-called feedback linearization (FL) methodology [2]–[4]. The FL control method, as applied to the IM, is based on the construction of two models expressing the dynamics of the rotor flux and the speed. Starting from the conventional model of the IM and by means of a nonlinear state feedback, two new models, consisting of a chain of two integrators supplied by a new auxiliary control variable and a total disturbance, are obtained. The total disturbance contains linear and nonlinear coupling terms, depending on the electromagnetic and mechanical parameters of the motor and load torque. Then, the control law is designed so as to compensate the above total disturbance, computed for rated parameters, in order to obtain the desired closed-loop dynamics. As a result, the control input is the superposition of a nonlinear function of the state and the auxiliary input. In absence of uncertainties, i.e., endogenous disturbances, the above nonlinear function, describing the disturbance, can be assumed known and, consequently, it can be suitably compensated. In the FL, however, the state-feedback computed analytically suffers from the problem arising from the uncertainties on both the dynamic model and its parameters. In some works, to overcome this problem, more complex models have been adopted [5], [6], or some parameters have been estimated online [7]–[9]. However, a way to overcome such a limitation of the FL, independently from the plant to be controlled, is the adoption of the so-called active disturbance rejection control (ADRC) [10]–[13]. The control method based on the active rejection of the disturbance can be viewed as an evolution of the state FL. As a matter of fact, in this method, the model of the system is led to an augmented model consisting of a chain of integrators in which the last equation expresses the

dynamics of the above-mentioned total disturbance. While in the classic FL method, this function is assumed known, in the ADRC method this function is estimated by means of an extended state observer (ESO), and then compensated. It follows that ADRC could be considered as a "robust version" of the FL control technique against parameter uncertainties, unmodeled dynamics, and exogenous disturbances, since the state feedback term is online estimated and then compensated. Recently, the ADRC was successfully employed in some applications such as sensorless control of permanent magnet synchronous motors [14], control of DC motors [15], magnetic bearing systems [16], and control of flywheel energy storage systems [17]. There are also recent contributions in the area of robotics and underactuated systems such as [18], [19]. Moreover, other application of the ADRC can be found in particular fields such as the suppression of the vibrations [20], or for tracking systems of micro/nanopositioning [21].

Nevertheless, few applications of this control methods to IMs have been provided by the scientific literature [22]–[25]. In particular, in [22], three control loops are designed according to the ADRC method, i.e., the speed, the quadrature current component, and the direct current component control loop. The actual rotor flux is assumed equal to its reference value, while the reference direct current component is obtained by dividing the reference rotor flux by the magnetizing inductance of the machine, thus avoiding the design, and implementation, of the rotor flux control loop. Obviously, this causes the loss of the robustness against the electromagnetic parameters, together with an uncertainty in the correct value of the reference quadrature current component. In [23], three first-order ADRC are designed for the speed and for the quadrature and direct current components, whereas for the rotor flux control loop, a conventional PI controller is employed. In [24], three ADRC controllers are designed, separately, for rotor flux, speed, and quadrature current component. The ADRC for rotor flux loop is designed starting from a model describing the dynamics of the rotor flux and the direct current component. The remaining two controllers are designed starting from the equations representing the dynamics of the speed and the quadrature current component. Differently from these papers, where a proportional-derivative controller is proposed, in [25] a linear controller is proposed in order to assign the desired dynamics to the speed and rotor flux of the linearized system.

However, two problems can deteriorate the performance of the ADRC method. These problems are caused by the estimation errors of the total disturbance and parameter variations that cannot be included into the endogenous disturbances and cannot be estimated by the ESO, such as the uncertainties in the knowledge of the forcing coefficient through which the control variable acts on the system. Such issues, to the best of the authors' knowledge, have never been addressed in the scientific literature. With the aim of achieving total robustness, this paper proposes an original solution to solve such critical aspects, based on the development of an advanced ADRC controller by adding a sliding-mode (SM) component to the control law designed for the ideal case [26]. The gain of the SM component is determined by imposing the sliding condition on the chosen sliding surface consisting of a linear combination of the tracking error and its derivative. The sliding condition is the same as the reaching condition of the sliding surface, and it is imposed by using the Lyapunov direct method. A rigorous Lyapunov-based analysis is proposed in order to give more intuitive guarantees of the convergence of the estimation error.

The proposed methodology has been tested by means of numerical simulations and experimental tests. In particular, it is shown that the basic ADRC fails when control gains uncertainties overcome certain bounds. In particular, it is shown that the basic ADRC is sensitive to the variation of inertia coefficient of the motor-load system, and this is a very common situation when a load is connected or disconnected. It is also shown that the proposed technique is robust against these situations, exhibiting a very good static and dynamic behaviors. Experimental comparisons between the basic ADRC and the proposed one are given in Section VII, to show the improvements achievable with the proposed ADRC upgrade. Moreover, experimental tests are carried out in very challenging operating conditions, such as contemporary variations of the speed and flux reference signals, and flux reference signal and load torque.

II. Dynamic Model of the IM

If the iron losses, the saturation of the electromagnetic circuit and the anisotropy of the geometric structure are neglected, the continuous-time mathematical model of the IM in the rotating rotor flux reference frame, in terms of the scaled rotor flux, is given by

$$\dot{i}_d = -a_{11}\, i_d + \left(\omega + a_{21}\frac{i_q}{\psi_d}\right) i_q + a_{12}\,\psi_d + c_1\, u_d \tag{1}$$

$$\dot{i}_q = -a_{11}\, i_q - \left(\omega + a_{21}\frac{i_q}{\psi_d}\right) i_d - c_1\,\omega\,\psi_d + c_1\, u_q \tag{2}$$

$$\dot{\psi}_d = a_{21}\, i_d - a_{22}\,\psi_d \tag{3}$$

$$\dot{\omega} = -a_m\,\omega + b_m\left(b_3\, i_q\,\psi_d - t_l\right) \tag{4}$$

$$\dot{\rho} = \omega + a_{21}\frac{i_q}{\psi_d} \tag{5}$$

where

$$a_{11} = \tfrac{1}{L_e}\left(R_s + \tfrac{L_s - L_e}{\tau_r}\right),\quad a_{12} = \tfrac{1}{\tau_r\, L_e},\quad a_{21} = \tfrac{L_s - L_e}{\tau_r}$$

$$a_{22} = \tfrac{1}{\tau_r},\quad c_1 = \tfrac{1}{L_e},\quad a_m = \tfrac{F}{J_m},\quad b_3 = \tfrac{2}{3}\,p,\quad b_m = \tfrac{p}{J_m}$$

and the symbols are defined in Table I.

Model (1)–(5) is useful for the field-oriented control method, because the control of the rotor flux appears decoupled from that of the speed; the first one is carried out by acting on the current i_d and the second by acting on the current i_q. However, the decoupling is only approximate, due to the high coupling of the dynamics of the two currents. This drawback can be overcome using the FL approach [2]–[8]. However, this kind of approach requires an exact knowledge of the model, and when there are uncertainties on the parameters, or unmodeled dynamics, the exact decoupling cannot be achieved. For this reason in this paper, a control law based on the ADRC method has been proposed, where the state-dependent feedback, which

TABLE I
LIST OF SYMBOLS

SYMBOLS	
i_d (i_q)	stator current component along d-axis (q-axis) of the rotor flux reference frame, A
ν_d (ν_q)	stator voltage component along d-axis (q-axis) of the rotor flux reference frame, V
ψ_d (ψ_q)	rotor flux along d-axis (q-axis) of the rotor flux reference frame, Wb
ω	rotor speed, rad/s
ρ	angle of the rotor flux space vector, rad
R_s (R_r)	stator [rotor] resistance, Ω
L_m (L_r) [L_s]	mutual (rotor) [stator] inductance, H
τ_r	$\left(=\frac{L_r}{R_r}\right)$ rotor time constant, s
L_e	$\left(=L_s-\frac{L_m^2}{L_r}\right)$ stator transient inductance H
F	viscous friction coefficient, N· ms
t_m (t_l)	motor (load) torque, N· m
J_m	inertia coefficient, N· ms^2
p	pole pairs

allows thus to be linearized the model, is suitably estimated by means of an ESO, avoiding problems originated from the inaccurate knowledge of the model itself.

III. ADRC CONTROL LAW

The ADRC approach is based on the construction of an extended model, of order $n+1$, where n is the order of the controlled system, by defining an additional state variable representing the total disturbance consisting of endogenous disturbances, external disturbances, and nonlinearities. The second step is the design of an ESO able to estimate the total disturbance. Finally, a control law is determined consisting of two components, the first compensates the total disturbance and the second assigns the desired behaviors.

A. Extended Models

Two distinct extended models are obtained starting from (1) to (5), i.e., the flux and the speed extended models. The first describes the dynamics of the rotor flux, and the other describes the dynamics of the speed.

1) Flux Extended Model: By defining $x_{\psi 1}=\psi_d$, and $x_{\psi 2}=\dot{\psi}_d$, it can be written that

$$\dot{x}_{\psi 1}=x_{\psi 2} \tag{6}$$

$$\dot{x}_{\psi 2}=f+b_\psi u_d \tag{7}$$

where the total disturbance f is given by

$$f=\left(a_{22}^2+a_{21}a_{12}\right)\psi_d-a_{21}\left(a_{22}+a_{11}\right)i_d+a_{21}\left(\omega+a_{21}\frac{i_q}{\psi_d}\right)i_q$$

and $b_\psi=a_{21}c_1$. By defining an extra state variable $x_{\psi 3}=f$, the flux extended model becomes

$$\dot{x}_{\psi 1}=x_{\psi 2} \tag{8}$$

$$\dot{x}_{\psi 2}=x_{\psi 3}+b_\psi u_d \tag{9}$$

$$\dot{x}_{\psi 3}=\dot{f}. \tag{10}$$

2) Speed Extended Model: The procedure used for obtaining the speed extended model is the same as the one used for the flux model. First of all, it is convenient to compute the derivative of the mechanical equation (4), obtaining

$$\ddot{\omega}=-a_m\dot{\omega}-b_m b_3\Big(\left(a_{11}+a_{22}\right)i_q+\omega\left(i_d+c_1\psi_d\right)\Big)\psi_d-b_m\dot{t}_l+c_1b_m b_3\psi_d u_q. \tag{11}$$

By defining $x_{\omega 1}=\omega$ and $x_{\omega 2}=\dot{\omega}$, the previous equation yields

$$\dot{x}_{\omega 1}=x_{\omega 2} \tag{12}$$

$$\dot{x}_{\omega 2}=\xi+b_\omega u_q \tag{13}$$

where $b_\omega=c_1b_m b_3\psi_d$, and ξ is the total disturbance defined as

$$\xi=-a_m\dot{\omega}-b_m b_3\Big(\left(a_{11}+a_{22}\right)i_q+\omega\left(i_d+c_1\psi_d\right)\Big)\psi_d-b_m\dot{t}_l.$$

Finally, defining a new state variable $x_{\omega 3}=\xi$, the following speed extended model is obtained:

$$\dot{x}_{\omega 1}=x_{\omega 2} \tag{14}$$

$$\dot{x}_{\omega 2}=x_{\omega 3}+b_\omega u_q \tag{15}$$

$$\dot{x}_{\omega 3}=\dot{\xi}. \tag{16}$$

Models (8)–(10) and (14)–(16) show that the flux and speed extended models have the same structure. Moreover, choosing the control variables as follows:

$$u_d=\frac{1}{b_\psi}\left(-\hat{x}_{\psi 3}+u_\psi\right) \tag{17}$$

$$u_q=\frac{1}{b_\omega}\left(-\hat{x}_{\omega 3}+u_\omega\right) \tag{18}$$

where $\hat{x}_{\psi 3}$ and $\hat{x}_{\omega 3}$ are the estimates of $x_{\psi 3}$ and $x_{\omega 3}$, respectively, the auxiliary control variables u_ψ and u_ω can be designed so that the speed and rotor flux can evolve according to the desired dynamics. The estimates of the total disturbances f and ξ (namely, $\hat{x}_{\psi 3}$ and $\hat{x}_{\omega 3}$) are made by means of two ESOs designed in order to estimate the state of the rotor flux and speed extended models.

Since the flux and speed models have the same structure, given by

$$\dot{x}_1=x_2 \tag{19}$$

$$\dot{x}_2=h+bu \tag{20}$$

then the extended models also have the same structure given by

$$\dot{x}_1=x_2 \tag{21}$$

$$\dot{x}_2=x_3+bu \tag{22}$$

$$\dot{x}_3=\dot{h} \tag{23}$$

where h and x_1 are the total disturbance and the output. Thus, it is convenient to focus on the general models (19) and (20) and (21)–(23).

Remark 1: Model (21)–(23) is an extended dynamic model, designed to estimate the equivalent disturbance h. Models (6)

and (7) and (12) and (13) represent a different way to describe the model (1)–(4), as two decoupled models making a different choice of the state variables. This transformation is needed in order to linearize exactly the model of the IM by means of a nonlinear state feedback (cf., [2]–[4]). This last nonlinear state feedback comes directly from the theory of the FL for nonlinear system, which allows, under certain conditions, a generic nonlinear model to be transformed into a chain of integrators by means of a diffeomorphic mapping. This technique is sensitive to the parameter variations, which represents its real limitation. What the authors want to achieve, as the main contribution of this paper, is exactly to make the controller robust against parameter uncertainties and load torque disturbances. The proposed ADRC with the addition of the SM action has the target to overcome this drawback. ⌟

B. ESO for a Third-Order Extended Model

The ESO chosen for the state estimation of model (21)–(23) is given by

$$\dot{\hat{x}}_1 = \hat{x}_2 - \epsilon g_1\left(\frac{\hat{x}_1 - x_1}{\epsilon^2}\right) \tag{24}$$

$$\dot{\hat{x}}_2 = \hat{x}_3 - g_2\left(\frac{\hat{x}_1 - x_1}{\epsilon^2}\right) + bu \tag{25}$$

$$\dot{\hat{x}}_3 = -\epsilon^{-1} g_3\left(\frac{\hat{x}_1 - x_1}{\epsilon^2}\right) \tag{26}$$

where ϵ is a suitable positive parameter, and the functions $g_i(\cdot)$, $i = 1, 2, 3$, can be chosen as either linear or nonlinear functions.

Defining the estimation errors

$$e_i = \hat{x}_i - x_i, \qquad i = 1, 2, 3 \tag{27}$$

and putting

$$\eta_i = \frac{e_i}{\epsilon^{3-i}}, \qquad i = 1, 2, 3 \tag{28}$$

the dynamics of variables η_i are described by the following equations:

$$\epsilon\dot{\eta}_1 = \eta_2 - g_1(\eta_1) \tag{29}$$

$$\epsilon\dot{\eta}_2 = \eta_3 - g_2(\eta_1) \tag{30}$$

$$\epsilon\dot{\eta}_3 = -\epsilon\dot{h} - g_3(\eta_1). \tag{31}$$

The structure of $g_i(\eta_1)$, $i = 1, 2, 3$, characterizes the structure of the ESO. In this paper, a linear ESO (LESO) has been employed. With this last choice, fixing $g_i(\eta_1) = \beta_i\eta_1$, $i = 1, 2, 3$, with β_i positive constants, (29)–(31) can be written as follows:

$$\epsilon\dot{\boldsymbol{\eta}} = \boldsymbol{A}\boldsymbol{\eta} + \epsilon\boldsymbol{b}\dot{h} \tag{32}$$

where $\boldsymbol{\eta} = \begin{bmatrix}\eta_1 & \eta_2 & \eta_3\end{bmatrix}^T$, and

$$\boldsymbol{A} = \begin{bmatrix} -\beta_1 & 1 & 0 \\ -\beta_2 & 0 & 1 \\ -\beta_3 & 0 & 0 \end{bmatrix}, \qquad \boldsymbol{b} = \begin{bmatrix} 0 \\ 0 \\ -1 \end{bmatrix}.$$

Now, the following theorem can be proven in order to show the stability of model (32). This fact is particularly important since the stability of model (32) implies the convergence of the estimation error as can be seen from (27) and (28).

Theorem 1: For $\epsilon > 0$, the state $\boldsymbol{\eta}$ of (32) converges into a ball centered in the origin, if matrix $\boldsymbol{A}$ is Hurwitz and if there exists a constant $M > 0$ such that $|\dot{h}| \leq M$.

Proof: The proof is given in the appendix. ■

The proof shown in the appendix follows the method shown [13], but with slightly different approach with respect of it. Indeed, it has been particularized to the case under study, involving directly the eigenvalues of $\boldsymbol{A}$. It should be highlighted that the stability of the ESO (29)–(31) for a generic Lipschitz nonlinear plant is proven also in [27].

Remark 2: A direct consequence of Theorem 1 is that the estimation errors also converge into ball centered in the origin, since from (27), (28), and (A-10) (see the proof of theorem given in the appendix), it holds

$$|e_i| \leq \nu\epsilon^{3-i} \qquad \forall t \geq \bar{t}(\gamma), \qquad i = 1, 2, 3. \tag{33}$$

⌟

Remark 3: Equation (33) shows that $|e_i|$ and $\bar{t}(\gamma)$ diminish while ϵ decreases, maintaining the same value of γ. It follows that the structure chosen for the LESO has a good performance, and ϵ is an important design parameter. The parameter ϵ has to be chosen as low as possible, considering that the lower ϵ, the lower the convergence time, the higher the bandwidth of the observer, and the lower the steady-state estimation errors. ⌟

The parameters β_i are computed so that the eigenvalues of the matrix $\boldsymbol{A}$ have a negative real part. In order to simplify the design, the three eigenvalues can be chosen real and coincident, considering the following characteristic polynomial of $\boldsymbol{A}$:

$$\Delta(\lambda) = \lambda^3 + \beta_1\lambda^2 + \beta_2\lambda + \beta_3 = (\lambda + \bar{\omega})^3 \tag{34}$$

where $\bar{\omega}$ is the bandwidth of the LESO.

C. Design of Flux and Speed Controllers

As already said, the flux and speed controllers present the same structure and can be designed using the same approach. With reference to (19) and (20), if $\hat{x}_3 \approx h$, the control law

$$u = \frac{1}{b}\left(-\hat{x}_3 + u_0\right) \tag{35}$$

leads to the model

$$\dot{x}_1 = x_2 \tag{36}$$

$$\dot{x}_2 = u_0 \tag{37}$$

which corresponds to a double integrator. This model is reachable and observable; consequently, a state feedback control law based on the assignment of the eigenvalues can be derived, but as it is well known, it does not allow us to obtain steady-state null errors. Consequently, in order to have perfect tracking of the constant reference, the state of model (36), (37) is augmented by a third variable z, whose dynamics is described as follows:

$$\dot{z} = x_{1\,\mathrm{ref}} - x_1 \tag{38}$$

where $x_{1\mathrm{ref}}$ is the desired value of x_1. As it is easy to verify, model (36)–(38) is reachable and the control law

$$u_0 = -\boldsymbol{k}^T \boldsymbol{x} \tag{39}$$

with $\boldsymbol{k} = \begin{bmatrix} k_1 & k_2 & k_3 \end{bmatrix}^T$ and $\boldsymbol{x} = \begin{bmatrix} x_1 & x_2 & z \end{bmatrix}^T$, allows to assign the eigenvalues of the dynamic matrix of the model. The characteristic polynomial of this matrix is given by

$$\Delta(\lambda) = \lambda^3 + k_1\lambda^2 + k_2\lambda + k_3 \tag{40}$$

where the parameters k_1, k_2, and k_3 can be determined assuming that the desired eigenvalues are $\lambda_1 = -\zeta\omega_n + j\omega_n\sqrt{1-\zeta^2}$, $\lambda_2 = -\zeta\omega_n - j\omega_n\sqrt{1-\zeta^2}$, and $\lambda_3 = \sigma$, where ω_n and ζ are the natural frequency and the damping factor, respectively, while σ is a negative real number. Obviously, the implementation of the above control law can be carried out using the state estimated by the ESO. More precisely, the implementation of the control law requires the knowledge of x_1 and x_2, whereas the knowledge of x_3 allows the total disturbance h to be compensated.

IV. Robust ADRC Control Law

The ADRC law is a good idea for the controller design of both linear and nonlinear uncertain systems. However, two intrinsic limits have to be addressed. Such limits are: 1) the deterioration of the performance of the ADRC control due to the estimation error of the total disturbance h; and 2) the uncertainty in the knowledge of the control gains b. Such issues have not been addressed explicitly in the scientific literature, to the best of the authors' knowledge.

With regard to the first problem, the estimation errors on h can occur for two reasons. The first is due to the fact that also in the ESOs the control u acts through the control gain b. The second is due to the fact that the estimate of the total disturbances is based on the signals ω and ψ_r, and both of these last two signals are unavoidably affected by uncertainties: the measurement of speed is corrupted by noise, and the ψ_r, which is estimated by an observer, strongly depends on the correctness of the adopted flux model (by including or not magnetic saturation, by including or not iron losses) as well as on the correct knowledge of its parameters (tuning of the flux model). Thus, if these two signals are affected by errors, the estimate of the ESOs will also be affected by errors. Looking at the ESO dynamics (24)–(26), it is apparent that $\hat{x}_1$ converges to x_1 independently of the model parameters, so from this point of view the ESO is very robust. However, x_1 represents the measured signal (in this case ω and ψ_r), and if x_1 is affected by errors, also $\hat{x}_1$ will converge to a wrong value. Consequently, x_2 and x_3 will also be affected by errors because derived from x_1 and $\hat{x}_1$. The approach shown in the following allows robustness to be gained also against the estimation errors of the disturbance given by the ESOs.

The second problem is connected to the fact that the control variable appears premultiplied by a parameter b, which depends on some parameters of the system together with the state variables. Obviously, in this case, the robustness against the parameter variations cannot be guaranteed, because the uncertainties on this term cannot be included into the endogenous disturbances and consequently cannot be estimated by means of the two ESOs. In [11], the case is considered in which the parameter b could be affected by uncertainties. More precisely, in [11, Sec. IV], it is assumed for b the rated value b_0 and its variations are considered in the range of $\pm 50\%$. However, this is not the case for the application under study, since here large variations, up to five times lower/higher than the rated (nominal) one, have been considered. This occurs particularly for speed control because b_ω depends on the moment of inertia, which can vary considerably when either a load is connected or disconnected, or during the conventional operations of the motor-load system (loading or discharging of conveyor belt, rolling mills, etc.). Note that this is a very common situation in practical applications. In such cases, an ad hoc procedure has to be considered, otherwise the control system will not be able to work correctly. In this paper, the robustness requirement is explicitly taken into account, and a procedure is described and justified from the theoretical point of view.

Moreover, in order to prove that the uncertainties on the parameter b cannot be compensated by means of the standard ADRC, the following considerations can be given. Let us consider the extended model (21)–(23). By means of the ESO (24)–(26), it is possible to estimate the variable x_3, namely, the equivalent disturbance h. Now, if the input u is chosen as in (35), while parameter b is uncertain ($b \in [b_m, b_M]$), then by defining the rated value of b, $\hat{b} = \sqrt{b_m b_M}$, the controlled model becomes

$$\dot{x}_1 = x_2 \tag{41}$$

$$\dot{x}_2 = h - \frac{b}{\hat{b}}\hat{x}_3 + \frac{b}{\hat{b}}u_0 \tag{42}$$

where $\hat{x}_3$ is an estimation of h given by ESO. If $\hat{b} = b$, then the above closed-loop system becomes the same as (36) and (37), but if $\hat{b} \neq b$, the following model is obtained:

$$\dot{x}_1 = x_2 \tag{43}$$

$$\dot{x}_2 = h\left(1 - \frac{b}{\hat{b}}\right) + \frac{b}{\hat{b}}u_0 \tag{44}$$

corresponding to the model

$$\dot{x}_1 = x_2 \tag{45}$$

$$\dot{x}_2 = \zeta + \frac{b}{\hat{b}}u_0 \tag{46}$$

where $\zeta = h\left(1 - \frac{b}{\hat{b}}\right)$. Now, for this kind of model, the disturbance ζ cannot be compensated, because in order to estimate ζ by an ESO the knowledge of $\frac{b}{\hat{b}}$ is needed, while the knowledge is only on $\hat{b}$. In other words, an ESO that estimates ζ cannot be implemented because $b/\hat{b}$ is unknown.

Moreover, in order to enforce this analysis, let us consider ζ as an extra disturbance input. If the superposition principle is applied, it is possible to investigate on the effects that ζ and u_0 produce when they act separately on the system. In particular, we are interested in the effects produced by u_0 when $b/\hat{b}$ varies

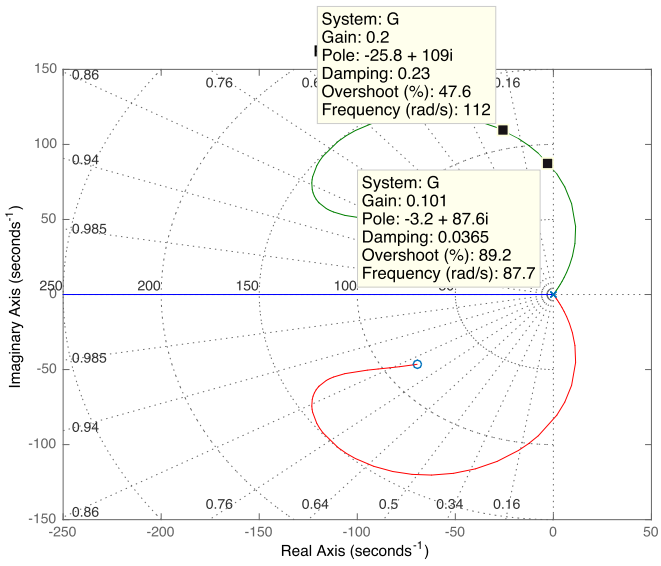

Fig. 1. Poles distribution of the closed-loop transfer function (49) when $b/\hat{b} \in [0,\ 1]$.

on a certain range. For this reason, let us consider the system

$$\dot{x}_1 = x_2 \tag{47}$$

$$\dot{x}_2 = \frac{b}{\hat{b}} u_0. \tag{48}$$

The transfer function of the closed-loop system (47), (48), with u_0 designed as in (39), is

$$W(s) = \frac{-k_3 \frac{\hat{b}}{b}}{s^3 + k_2 \frac{\hat{b}}{b} s^2 + k_1 \frac{\hat{b}}{b} s - k_3 \frac{\hat{b}}{b}} \tag{49}$$

where k_3 is negative.

Note that (49) represents the transfer function of the closed-loop system when the classic ADRC with pole assignment is used. The poles distribution of (49) are the roots of the equation

$$1 + \frac{b}{\hat{b}} \frac{k_2 s^2 + k_1 s - k_3}{s^3} = 0. \tag{50}$$

Fig. 1 represents the root locus of (50) as a function of $\frac{b}{\hat{b}}$, with $b/\hat{b} \in [0,\ 1]$ and parameters k_1, k_2, and k_3 considered as in Section V (note that $b/\hat{b} \in [0,\ 1]$ represents the situation when the inertia moment increases).

Note that the form and the graduation in $b/\hat{b}$ of the locus strongly depends on the parameters of the controller, i.e., k_1, k_2, and k_3, which depends on the poles assigned to the closed-loop system.

Looking at Fig. 1, it can be clearly noted that there exist some values of $b/\hat{b}$ for which the poles of the closed-loop system present a positive real part, that is in working conditions in which the system becomes unstable. Moreover, also if the poles of the closed-loop system are with negative real part, it is possible to see that the damping factor becomes very low when $b/\hat{b}$ becomes less than 0.3–0.4. Fig. 1 shows the case of $b/\hat{b} = 0.2$, corresponding to an increment as much as five times the inertia moment with respect to its rated value. In this case, the damping factor of the two complex conjugate poles becomes 0.23, which cannot be tolerated in many industrial applications. The distribution for $b/\hat{b} > 1$ is not shown because all the poles are with negative real part, and the damping factor is greater than 0.8, so no problems occur when $b > \hat{b}$. This analysis confirms that, for very large uncertainties of coefficient b, stability problems can occur in the real system, and it better explains the simulation results given in Section V.

Starting from the above considerations, the basic ADRC has been upgraded adding an SM control component to the already designed control law (39), to overcome the two above cited limits.

Assumption 1: It is assumed that the maximum error between h and its estimate $\hat{h}$ is

$$\left|\tilde{h}\right| = \left|h - \hat{h}\right| \leq \epsilon_h \left|\hat{h}\right|. \tag{51}$$

Moreover, it is assumed that $b \in [b_m, b_M]$, where b_m and b_M are the minimum and the maximum value, respectively, of the parameter b. Assuming $\hat{b} = \sqrt{b_m b_M}$ and $\beta = \sqrt{b_M / b_m}$, it follows that

$$\frac{b}{\hat{b}} \in [\beta^{-1}, \beta]. \tag{52}$$

See [26] for further details. ⌟

Now the following theorem, developed in this paper for the case under study, can be given.

Theorem 2: For the system (19), (20), let us define the input u as follows:

$$u = \frac{1}{\hat{b}}\left(- \hat{h} + u_0 + u_{\text{SM}}\right) \tag{53}$$

$$u_{\text{SM}} = -\kappa\, \text{sign}(s) \tag{54}$$

$$s = \dot{e} + \chi e \tag{55}$$

where $\chi > 0$ is a suitably chosen constant, s is the sliding surface, $e = x_1 - x_{1,\text{ref}}$, and u_0 is the control input (39) designed in the ideal case of perfect knowledge of h and b. If the gain κ is designed as follows:

$$\kappa = \left|u_0 - \hat{h}\right| + \beta\epsilon_h \left|\hat{h}\right| + \beta\left|\hat{h} + \chi(x_2 - \dot{x}_{1,\text{ref}}) - \ddot{x}_{1,\text{ref}}\right| \tag{56}$$

then the sliding condition is verified and the system slides on the surface $s = 0$, for each values of the uncertainties satisfying Assumption 1.

Proof: Substituting (53) into (20), we have

$$\dot{x}_2 = \left(h - \frac{b}{\hat{b}}\hat{h}\right) + \frac{b}{\hat{b}}\left(u_0 - \kappa\, \text{sign}(s)\right). \tag{57}$$

Now, let us define the Lyapunov candidate function as follows:

$$V(s) = \frac{1}{2} s^2. \tag{58}$$

Computing the derivative of (58), we obtain $\dot{V}(s) = s\dot{s}$ and, consequently, for obtaining $\dot{V}(s) < 0$, the following sliding

conditions have to be satisfied:

$$\begin{cases} \dot{s} > 0, & \text{for } s < 0 \\ \dot{s} < 0, & \text{for } s > 0. \end{cases} \tag{59}$$

From (54) and (55), we have

$$\begin{aligned} \dot{s} &= \dot{x}_2 - \ddot{x}_{1,\text{ref}} + \chi(x_2 - \dot{x}_{1,\text{ref}}) \\ &= \tilde{h} + \left(1 - \frac{b}{\hat{b}}\right)\hat{h} + \frac{b}{\hat{b}}\left(u_0 - \kappa\,\text{sign}(s)\right) \\ &\quad + \chi(x_2 - \dot{x}_{1,\text{ref}}) - \ddot{x}_{1,\text{ref}}. \end{aligned} \tag{60}$$

Then, from (59), it is obtained that

$$\tilde{h} + \left(1 - \frac{b}{\hat{b}}\right)\hat{h} + \frac{b}{\hat{b}}(u_0 - \kappa) + \chi(x_2 - \dot{x}_{1,\text{ref}}) - \ddot{x}_{1,\text{ref}} < 0, \quad \text{for } s > 0 \tag{61}$$

$$\tilde{h} + \left(1 - \frac{b}{\hat{b}}\right)\hat{h} + \frac{b}{\hat{b}}(u_0 + \kappa) + \chi(x_2 - \dot{x}_{1,\text{ref}}) - \ddot{x}_{1,\text{ref}} > 0, \quad \text{for } s < 0 \tag{62}$$

both of which are satisfied for

$$\kappa > \max_{\tilde{h},b} \left| u_0 - \hat{h} + \frac{\hat{b}}{b}\left(\tilde{h} + \hat{h} + \chi(x_2 - \dot{x}_{1,\text{ref}}) - \ddot{x}_{1,\text{ref}}\right)\right|. \tag{63}$$

Using the conditions given in Assumption 1, (63) can be maximized as follows:

$$\begin{aligned} &\left| u_0 - \hat{h} + \frac{\hat{b}}{b}\left(\tilde{h} + \hat{h} + \chi(x_2 - \dot{x}_{1,\text{ref}}) - \ddot{x}_{1,\text{ref}}\right)\right| \\ &\le \left|u_0 - \hat{h}\right| + \frac{\hat{b}}{b}\left|\tilde{h}\right| + \frac{\hat{b}}{b}\left|\hat{h} + \chi(x_2 - \dot{x}_{1,\text{ref}}) - \ddot{x}_{1,\text{ref}}\right| \\ &\le \left|u_0 - \hat{h}\right| + \beta\epsilon_h\left|\hat{h}\right| + \beta\left|\hat{h} + \chi(x_2 - \dot{x}_{1,\text{ref}}) - \ddot{x}_{1,\text{ref}}\right|. \end{aligned} \tag{64}$$

From (64), it follows that (59) is satisfied if

$$\kappa = \left|u_0 - \hat{h}\right| + \beta\epsilon_h\left|\hat{h}\right| + \beta\left|\hat{h} + \chi(x_2 - \dot{x}_{1,\text{ref}}) - \ddot{x}_{1,\text{ref}}\right|. \tag{65}$$

QED. ■

Theorem 2 is particularly important since it gives a rigorous procedure in order to design a robust control input addressing the problems introduced to the beginning of this section, when parameter $b/\hat{b}$ varies in the range (52), and the maximum error $|\tilde{h}|$ of h satisfies (51). Moreover, the presented conditions are suitably developed in this paper, for the considered application.

Remark 4: From the proof of Theorem 2, it is evident that two procedures can be followed in order to satisfy condition (63). The first consists of the estimation of a upper bound of κ, which satisfies the sliding condition in all the possible operating situations, and the second consists of the choice of a time-varying value of κ considering the maximum variation of the parameters, and the actual values of the state variables, estimated or measured, in a particular working condition. The first choice is too conservative and results in increasing of the chattering. The second choice has been adopted in this paper. Moreover, it is useful to note that even if the gain is time varying, it does not depend on the particular values of b or h which are unknown, but it considers only the estimate $\hat{h}$, the maximum error between h and $\hat{h}$, and the maximum value of $b/\hat{b}$ given in Assumption 1. ⌟

Remark 5: The control gains b_ψ and b_ω depend on the parameters of the IM model. In particular, b_ψ depends on the electromagnetic parameters, whereas b_ω depends on the magnetic and mechanical parameters, and on the rotor flux ψ_d and, consequently, it is a function of a state variable. They do not depend on the total disturbances ξ and f, which include endogenous and exogenous disturbances. Consequently, the effects of the total disturbances and those due to the uncertainties in the knowledge of b_ψ and b_ω can be addressed separately. This has been exactly the approach in this paper. More precisely, the total disturbances, assumed as absolutely uniformly bounded, are estimated by two ESOs and then compensated by means of (17) and (18), assuming a perfect knowledge of b_ψ and b_ω. Then, in order to improve robustness, it is assumed that estimation errors of the two total disturbances occur, together with uncertainties in the knowledge of the two control gains. These uncertainties are also assumed bounded. The robustness is achieved by adding to both the rotor flux and the speed loops two SM components. Each of them is designed in a simple way because, as already said, total disturbances and uncertainties in the control gains can be treated separately, and only the upper bounds of the errors have been considered. An alternative way, with respect to the sliding component, could be to estimate adaptively the control gains b_ψ and b_ω. However, in this case, a special approach (much more difficult to prove, and with a consequent increase of the computational burden) has to be devised. This last option has not been addressed in this paper, since it is out of its current scope, while it can be followed as a future development of this paper. ⌟

TABLE II
PARAMETERS AND RATED DATA OF THE MOTOR

L_s	0.2030 H	τ_r	0.135 s	Rated power	2.2 kW
L_e	0.01798 H	J_m	0.0088 N · ms^2	Rated torque	14.9 N · m
R_s	2.9 Ω	F	0.0023 N · ms	Pole pairs	2

V. SIMULATION RESULTS

The proposed control techniques have been tested by means of numerical simulations in MATLAB-Simulink environment. The Simulink model includes the ADRC control law, the two ESOs, and the IM model. The IM model used for the simulation tests is the same as the one used in the experimental tests, whose parameters and rated data are shown in Table II.

The parameters of the ESOs and controllers are given below.

A. Flux Model

The ESO for flux is designed with $\epsilon = 0.02$ and with parameters $\beta_i = \beta_{\psi i}$, for $i = 1, 2, 3$, chosen such that (34) is satisfied with $\bar{\omega} = \omega_\psi = 40$ rad/s. The control law is given by (17) with $u_\psi = \boldsymbol{k}_\psi^T \boldsymbol{x}_\psi$, where $\boldsymbol{k}_\psi$ is determined so that the zeros λ_1, λ_2, and λ_3 of the polynomial (40) are chosen with $\omega_n = 150$ rad/s, $\zeta = 0.9$, and $\sigma = -400$. The state is $\boldsymbol{x}_\psi = \begin{bmatrix} x_{\psi_1} & x_{\psi_2} & z_\psi \end{bmatrix}^T$ in which z_ψ is the output of an integrator supplied by the flux tracking error $\left(\psi_{d\,\mathrm{ref}} - x_{\psi\,1}\right)$.

B. Speed Model

The ESO for speed is designed with $\epsilon = 0.02$ and with parameters $\beta_i = \beta_{\omega i}$, for $i = 1, 2, 3$, chosen such that (34) is satisfied with $\bar{\omega} = \omega_\omega = 40$ rad/s. The control law is given by (18) with $u_\omega = \boldsymbol{k}_\omega^T \boldsymbol{x}_\omega$, where $\boldsymbol{k}_\omega$ is determined so that the zeros λ_1, λ_2, and λ_3 of the polynomial (40) are chosen with $\omega_n = 100$ rad/s, $\zeta = 0.9$, and $\sigma = -400$. The state is $\boldsymbol{x}_\omega = \begin{bmatrix} x_{\omega_1} & x_{\omega\,2} & z_\omega \end{bmatrix}^T$ in which z_ω is the output of an integrator supplied by the speed tracking error $(\omega_{\mathrm{ref}} - x_{\omega\,1})$.

With regard to the SM component (54), it has been designed assuming a slope of the sliding surface χ equal to $\chi = 0.2$, and condition (56) has been computed assuming $\epsilon_h = 0.2$ for both speed and rotor flux loops, while $b_m = 0.5 \cdot \hat{b}$ and $b_M = 2 \cdot \hat{b}$ for the rotor flux loop, and $b_m = 0.2 \cdot \hat{b}$ and $b_M = 5 \cdot \hat{b}$ for the speed loop.

A further comment is that there is not a closed-loop control of the stator currents. The absence of a closed-loop control of the stator currents is typical of all state-feedback controllers, for example, the input–output FL. As a matter of fact, the idea is to control, with the best achievable dynamic performance, the speed and the rotor flux of the IM, while the stator currents are considered as internal dynamic and their values can be indirectly bounded by means of a suitable choice of the controller parameters (i.e., by means of a suitable choice of the bandwidth of the controller which has been fixed at 100 rad/s for the speed loop, and at 150 rad/s for the flux loop in the case under study), in order to avoid potential damages of the system. Alternatively, in order to maintain the stator currents within the bounds allowed by the data sheets of the motor, particular attention has been paid to the choice of the speed and rotor flux reference waveforms, avoiding step signals and considering acceleration/deceleration ramps. In this context, convenient nonlinear differentiators can be designed in order to generate smooth reference of speed and rotor flux [24].

As simulation test, the machine is fluxed at zero reference speed up to 1 s, and then, it is started with reference speed of 150 rad/s; finally, a load torque of 15 N· m is applied at 2 s. In this test, the inertia is increased four times with respect to the rated value in order to highlight the effectiveness of the followed approach.

Fig. 2 shows the angular speed during the above described test. It is evident that when the inertia is increased of four times with respect to the rated value, the behavior of the overall control system, controlled with the basic ADRC, is at the limit of the stability, while when the proposed robust approach is used the system tracks its reference very well. Also, the rotor flux, shown in Fig. 3, becomes oscillating when the speed is different from zero and the basic ADRC is used, while it behaves well with the proposed robust approach. These results not only show the effectiveness of the followed approach, but also confirm the analysis carried out on Section IV about the large variations of the parameter b.

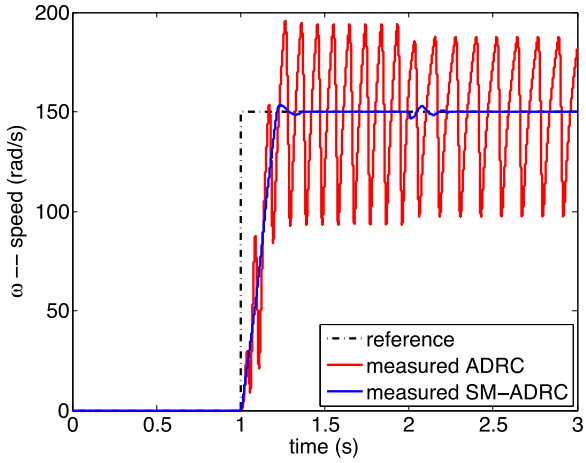

Fig. 2. Angular speed during a simulation test.

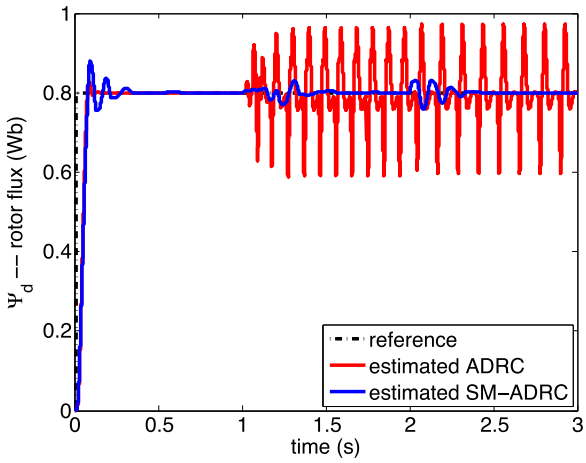

Fig. 3. Rotor flux amplitude during a simulation test.

In order to better understand how much these oscillating behaviors are related with the controller or with the ESO, a different simulation test has been carried out. In particular, the SM components have been removed, and the ESOs have been also excluded when computing analytically the total disturbance. This test is performed with the aim of analyzing the behavior of the system (47), (48), i.e., when only a variation of the control gain occurs, assuming that the total disturbance is perfectly compensated (since it has been analytically computed). Moreover, the inertia is increased of four times as in the above test, leading the system to the part of the locus with very low damping factor (0.23). Figs. 4 and 5 show that both the angular speed and the rotor flux exhibit an oscillatory behavior, also when the total disturbance is perfectly compensated and the feedback occurs on the computed state variables. Consequently, the oscillating

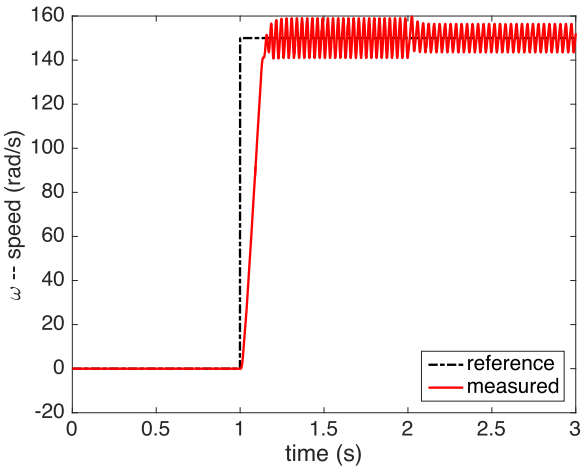

Fig. 4. Angular speed during a simulation test with total disturbance perfectly compensated and control gain increased of four times with respect to the rated value.

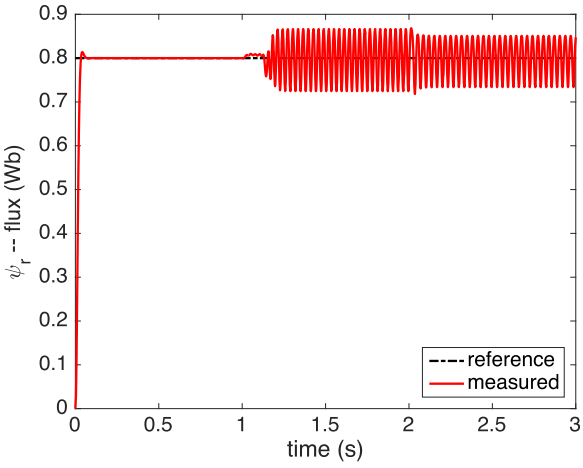

Fig. 5. Rotor flux during a simulation test with total disturbance perfectly compensated and control gain increased of four times with respect to the rated value.

behaviors are due to the controller, and to the fact that by increasing the inertia moment, the instability region is approached where the damping factor is very low. Obviously, in this case, the oscillations are smaller than the previous test (see Figs. 2 and 3), because in the test shown in Figs. 2 and 3, the ESO was considered in the loop, and these oscillating waveforms were injected into the loop by the ESOs, amplifying the effects (note the ESOs are sourced by the measured flux and speed signals). Instead, including the SM components into the controller, both the ripple in the speed and the ripple in the rotor flux disappear.

Obviously, due to the stability problems, these tests cannot be reproduced experimentally. The other tests, under rated conditions, will be shown experimentally in Section VI.

Remark 6: Note that the locus in Fig. 1 strongly depends on the parameters of the controller, i.e., k_1, k_2, and k_3, which depend on the poles assigned to the closed-loop system. So, probably, increasing such parameters, i.e., the modulus of the poles assigned to the speed and rotor flux loops, by the increase of the bandwidth of the system, it could be possible to find a set of parameters that limit the above oscillating behavior. However, an increment of the bandwidth leads to an increment of the effects of noise on the variables of the system, and also an increment of the value of the stator current during transient since, as already said, it is considered as internal dynamic and its value is indirectly bounded by means of the suitable choice of the bandwidth of the controller.

The drawback is a more complex algorithm from the computational point of view, because two additional SM components must be computed, and the presence of chattering induced by these control components in the variables of system, namely in the stator voltages. However, the proposed method represents a systematic procedure in order to take explicitly into account the robustness requirements. ⌟

VI. Experimental Setup

A test setup has been suitably built to validate the proposed control technique. The machine under test is a 2.2 kW IM SEIMEC model HF 100LA 4 B5, equipped with an incremental encoder. The employed test setup consists of:

1) a three-phase 2.2 kW IM; the parameters and the rated data of the motor are shown in Table II;
2) a frequency converter that consists of a three-phase diode rectifier and a 7.5 kVA three-phase VSI;
3) one electronic card with voltage sensors (model LEM LV 25-P) and current sensors (model LEM LA 55-P);
4) a dSPACE card (DS1103) with a PowerPC 604e at 400 MHz and a fixed-point DSP TMS320F240.

The test setup is equipped with a torque-controlled PMSM model Emerson Unimotor FM mechanically coupled to the IM, to implement an active load for the IM. The electromagnetic torque is measured on the shaft by a torquemeter model Himmelstein 59 003 V. The whole system, consisting of the two controllers, the two ESOs, and the flux observer designed as in [28], is processed at 12 kHz.

The parameters of the ESOs, of the controllers, and of the SM components are designed as shown in Section V.

VII. Experimental Results

Experimental results show the improvements achievable with the described robust ADRC.

Figs. 6(a), 7(a), and 8(a) show the experimental waveforms of angular speed, rotor flux, and i_d and i_q stator current components during a speed reversal test at no load. Fig. 6(a) shows that the robust ADRC works better than the conventional one, especially during transients. The robust ADRC gives lower rise and settling times and overshoot. The higher rise time shown in Fig. 6(a) is also justified by the waveform of the i_q current, consequent to the speed reversal command, shown in Fig. 8(a). Figs. 7(a) and 8(a) show the waveforms of the rotor flux and i_d current. These waveforms are coherent with the comments made above. The i_d current corresponding to the robust ADRC displays a higher dynamics, and this produces a more regular waveform of the rotor flux, as it appears in Fig. 7(a). These results are confirmed

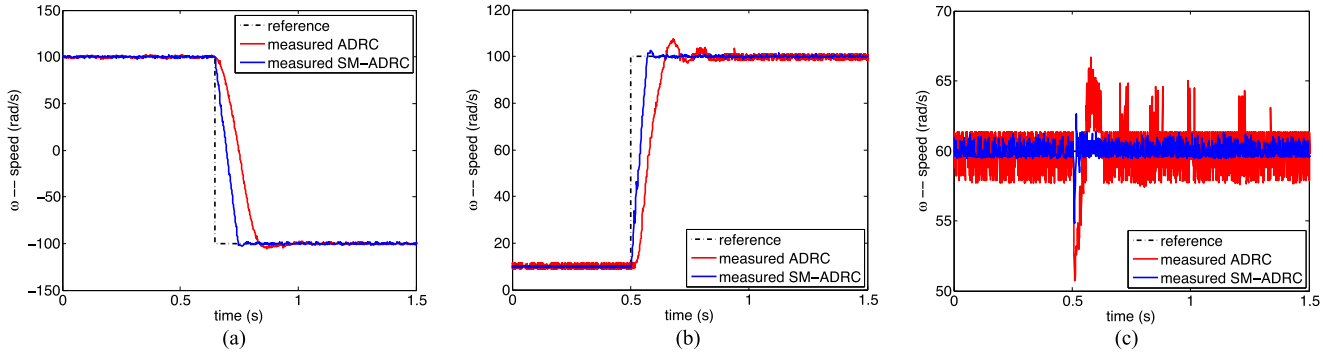

Fig. 6. Angular speed during the (a) speed reversal test, during a (b) contemporary flux and speed variation test, and during a (c) contemporary flux and torque variation test (experiment).

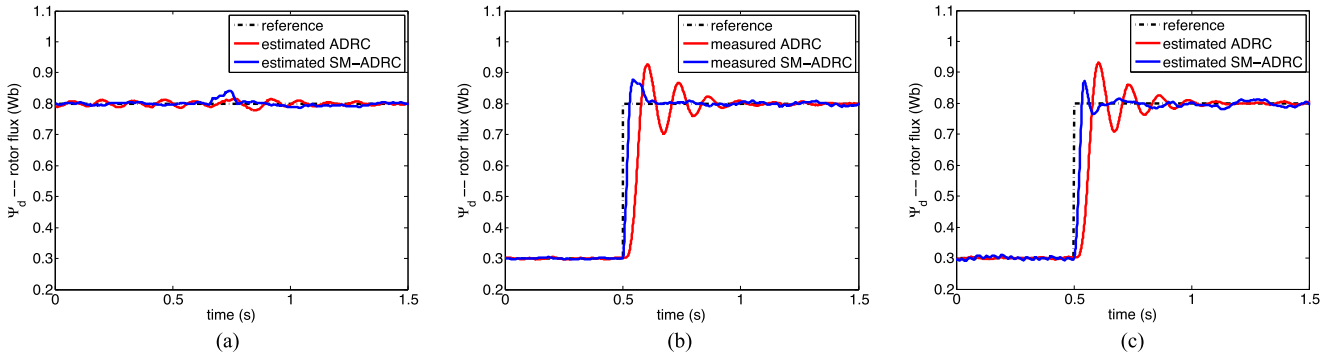

Fig. 7. Rotor flux amplitude during the (a) speed reversal test, during a (b) contemporary flux and speed variation test, and during a (c) contemporary flux and torque variation test (experiment).

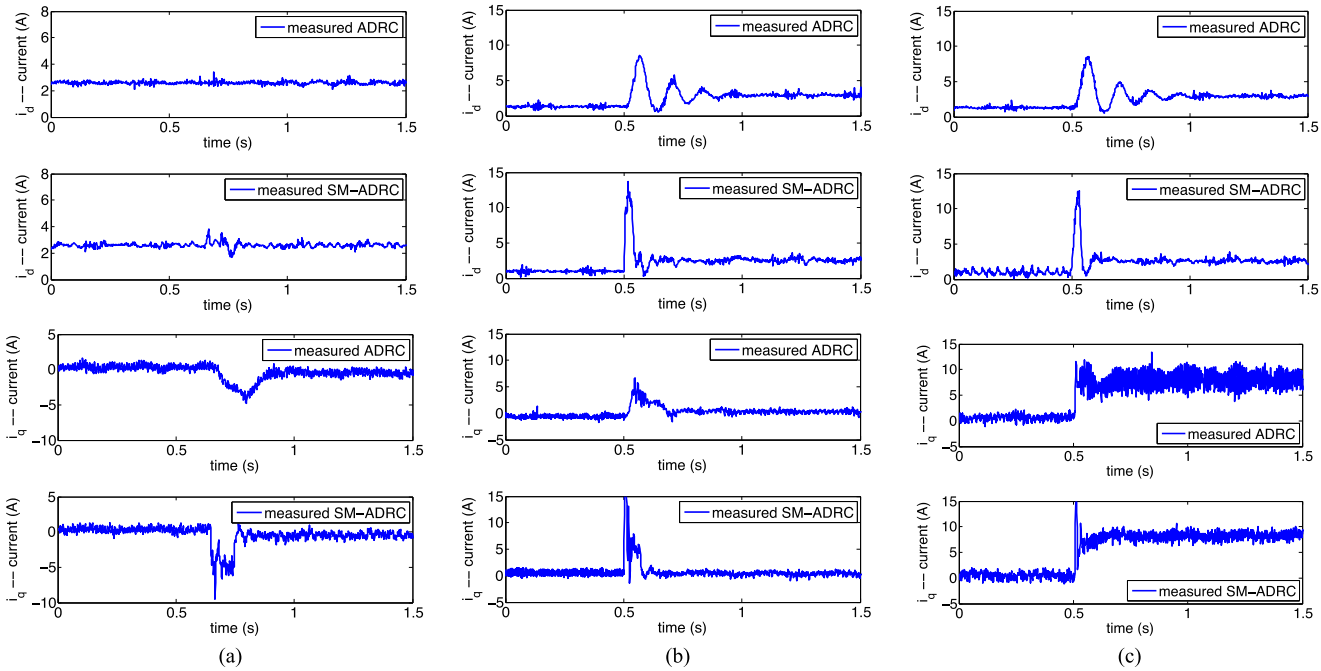

Fig. 8. i_d and i_q stator current components during the (a) speed reversal test, during a (b) contemporary flux and speed variation test, and during a (c) contemporary flux and torque variation test (experiment).

TABLE III
PERFORMANCE INDEXES

	Speed reversal test		Flux and speed variation test		Flux and torque variation test	
	ADRC	SM-ADRC	ADRC	SM-ADRC	ADRC	SM-ADRC
Speed tracking error: $\int_0^T \left\|\omega(t) - \omega_{\mathrm{ref}}(t)\right\| dt$	21.26	10.6	8.324	3.599	1.820	0.509
Flux tracking error: $\int_0^T \left\|\psi_d(t) - \psi_{d\,\mathrm{ref}}(t)\right\| dt$	0.00933	0.00834	0.0455	0.0215	0.0451	0.0164

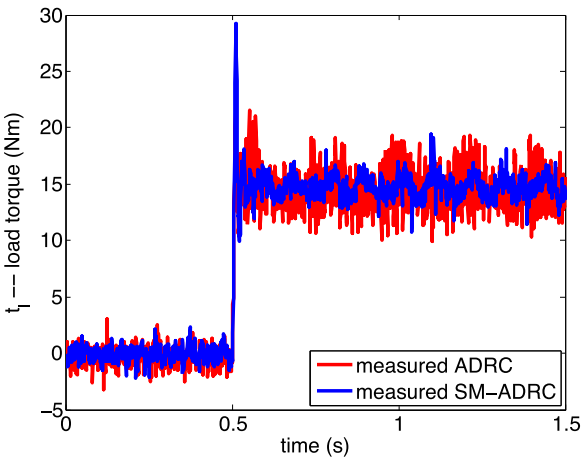

Fig. 9. Measured load torque during a contemporary flux and torque variation test (experiment).

in Table III, where the index integral absolute error (IAE) is computed during the whole tests in the figures themselves.

Another meaningful test is that one illustrated in Figs. 6(b), 7(b), and 8(b), consisting of simultaneous commands of reference speed and rotor flux, starting from a steady-state situation corresponding to a reference speed of 10 rad/s and a rotor flux of 0.3 Wb. The responses of the speed and rotor flux are faster than those relative to the conventional ADRC and, moreover, the robust ADRC forces the motor–load system to the new steady state rapidly and without any oscillations [cf., Figs. 6(b) and 7(b)]. These responses are justified by the waveforms of the i_d and i_q currents [cf., Fig. 8(b)], where it is well evident the effectiveness of the robust ADRC in both the fast response and the reduction of the number of oscillations before reaching the steady state. Also, during this test, the IAE indexes, shown in Table III, confirm the effectiveness of the robust ADRC.

In Figs. 6(c), 7(c), 8(c), and 9, the behavior of the whole control system consequent to simultaneous variation of both the rotor flux from 0.3 to 0.8 Wb, as in the previously described test, and the load torque from 0 N· m to the rated torque of 15 N· m, at a speed of 60 rad/s. Fig. 6(c) shows clearly that the robust ADRC forces the system to recover the steady-state operation in a lower time and with maximum positive and negative variations smaller than the conventional ADRC. It is useful to note that although the noise of the red signal in Fig. 6 is bigger than the blue signal, this effect is not due to the chattering since the red signal refers to ADRC control, without the addiction of the SM components, while the blue signal refers to ADRC control with the addiction of the SM components. This reduction in the oscillations of the controlled variables is due to a more accurate and faster control action.

Fig. 7(c) shows the waveform of the rotor flux that confirms the same considerations already formulated in the previously described tests. Finally, Fig. 9 shows the waveform of the measured load torque, which is the maximum admissible (15 N· m) for the machine under test.

Fig. 10 shows the supply voltage for the three above described tests with the robust ADRC. From these figures, the presence of the sliding components in the stator voltages is evident, especially in the low-frequency part of the test.

Finally, the sliding surfaces s and the product $s\dot{s}$ have been shown in Fig. 11, and the waveforms of the gains (56) of the SM components have been shown in Fig. 12. In particular, the top plots show the waveforms of s in (55) for the three above described tests with the robust ADRC. It is evident that the condition $s = 0$ is satisfied at steady state, so the system slides on the chosen surfaces and it correctly tracks the references. Moreover, in the bottom plots, it is shown that the sliding condition $s\dot{s} < 0$ is always satisfied.

An important remark should be done about the chattering. Surely, the price of the proposed solution is the presence of chattering induced in the control variables of system, namely, in the stator voltages. There exist many possible solutions to address this problem, such us the method based on the boundary layer, or equivalent techniques that decrease suitably the SM gain when the system approaches to the steady state. However, in the application under study, none of these techniques has been applied because the chattering in the controlled variables is not observable for the following three reasons.

1) With regard to the rotor flux amplitude control, its on-line estimation has been performed by adopting a full-order state observer designed as in [28], which filters the high-frequency measurement noise and consequently reduce the chattering; independently of it, the dynamics of the rotor flux amplitude is governed by the rotor time constant $1/a_{22}$, and thus, it introduces naturally a filtering action. Obviously, the bandwidth of this natural filter action is lower than the bandwidth of the flux observer, so that no artificial limitations about the dynamic performance of the machine are introduced.
2) With regards to the speed, the chattering is reduced due to the inertia of the motor-load system, which inherently behaves as a low-pass filter with a time constant $1/a_m$.

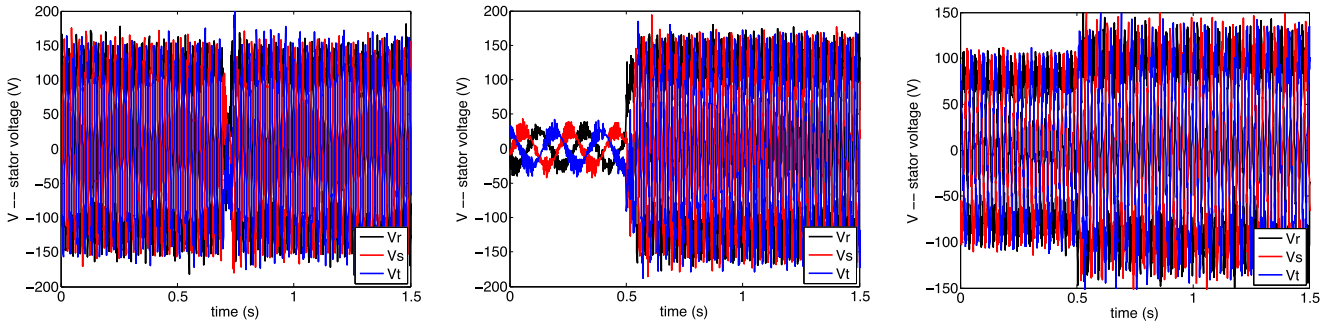

Fig. 10. Three-phase stator voltages with the SM-ADRC, during the (a) speed reversal test, during a (b) contemporary flux and speed variation test, and during a (c) contemporary flux and torque variation test (experiment).

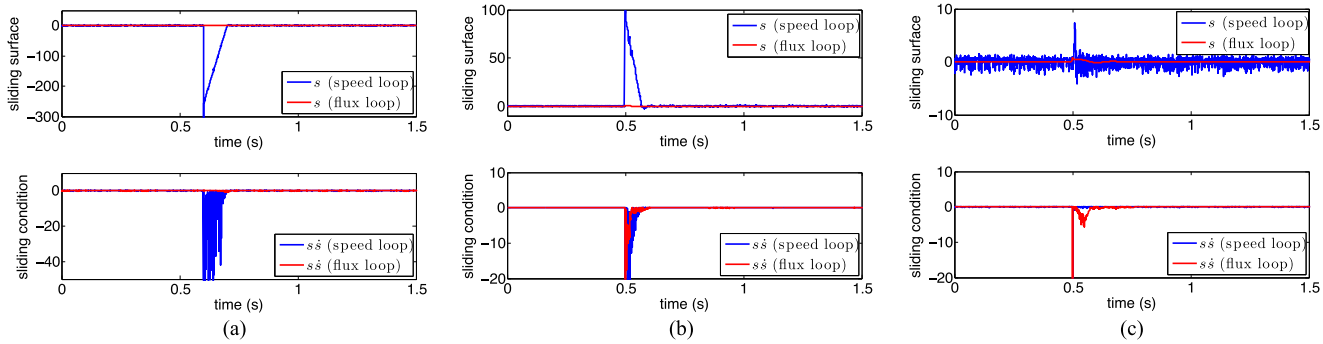

Fig. 11. Sliding surface s and sliding condition $s\dot{s}$ with the SM-ADRC, during the (a) speed reversal test, during a (b) contemporary flux and speed variation test, and during a (c) contemporary flux and torque variation test (experiment).

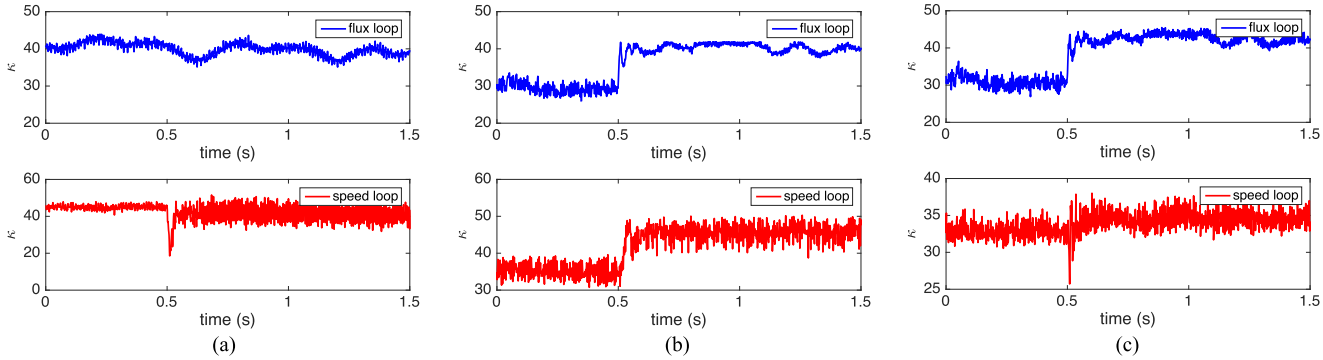

Fig. 12. Gain of the SM components, during the (a) speed reversal test, during a (b) contemporary flux and speed variation test, and during a (c) contemporary flux and torque variation test (experiment).

3) The commutation frequency is 12 kHz, as indicated in Section VI, so the corresponding chattering appearing in the stator voltages is also with a frequency of 12 kHz, which is much higher than the time constants of the speed and of the flux indicated at point 1) and 2), and consequently the chattering is filtered in the output variables.

For these reasons, the control law can be implemented in the form described in this paper. The experimental results carried out on the 2.2 kW prototype show clearly that this is possible. Looking at Figs. 6 and 7, it is possible to see that the results obtained with the SM-ADRC controller produce a better performance in terms of speed variation at steady state than the ADRC controller. Moreover, the results show that the chattering obtained with SM-ADRC is less than 1%, which is widely tolerable in a lot of practical applications.

VIII. Conclusion

This paper proposed a robust version of the ADRC control law. In particular, it proposed a solution for overcoming two serious limits of the classic ADRC: 1) the uncertainty in the knowledge of the control gains; and 2) the deterioration of the performance of the ADRC control due to the non-null estimation error of the total disturbance. In order to address these limits, a SM component had been added to the control law obtained for the basic ADRC. It is shown that the proposed procedure

is crucial when high variations of the IM parameters are to be expected, in particular as far as the inertia is concerned. The proposed robust ADRC was tested in numerical simulation and experimentally on a suitably devised test setup. The experimental results show the improvements achievable by the robust ADRC, especially in case of highly varying system parameters. In fact, the proposed procedure allows us to reduce the rise time, the overshoot, and the settling time of the controlled variables, i.e., the speed and the rotor flux, keeping the stator currents bounded.

APPENDIX

A. Proof of Theorem 1: If $\boldsymbol{A}$ is Hurwitz, there exist two symmetric positive-definite matrices $\boldsymbol{P}$ and $\boldsymbol{Q}$ such that $\boldsymbol{A}^T\boldsymbol{P}+\boldsymbol{P}\boldsymbol{A}=-\boldsymbol{Q}$. Let us define the scalar function $V(\boldsymbol{\eta})=\boldsymbol{\eta}^T\boldsymbol{P}\boldsymbol{\eta}\geq 0$, with $V(\boldsymbol{\eta})=0$ only if $\boldsymbol{\eta}=0$. Then, using (32), we have

$$\dot{V}(\boldsymbol{\eta})=2\boldsymbol{\eta}^T\boldsymbol{P}\dot{\boldsymbol{\eta}}=\frac{1}{\epsilon}\left(\boldsymbol{\eta}^T\left(\boldsymbol{A}^T\boldsymbol{P}+\boldsymbol{P}\boldsymbol{A}\right)\boldsymbol{\eta}+2\epsilon\dot{h}\boldsymbol{\eta}^T\boldsymbol{P}\boldsymbol{b}\right)$$
$$=-\frac{1}{\epsilon}\boldsymbol{\eta}^T\boldsymbol{Q}\boldsymbol{\eta}+2\dot{h}\boldsymbol{\eta}^T\boldsymbol{P}\boldsymbol{b}=-\frac{W(\boldsymbol{\eta})}{\epsilon}+2\dot{h}\boldsymbol{\eta}^T\boldsymbol{P}\boldsymbol{b} \tag{A-1}$$

where $W(\boldsymbol{\eta})=\boldsymbol{\eta}^T\boldsymbol{Q}\boldsymbol{\eta}\geq 0$. The functions $W(\boldsymbol{\eta})$ and $V(\boldsymbol{\eta})$ satisfy the following conditions:

$$\lambda_m(\boldsymbol{P})||\boldsymbol{\eta}||^2\leq V(\boldsymbol{\eta})\leq\lambda_M(\boldsymbol{P})||\boldsymbol{\eta}||^2 \tag{A-2}$$
$$\lambda_m(\boldsymbol{Q})||\boldsymbol{\eta}||^2\leq W(\boldsymbol{\eta})\leq\lambda_M(\boldsymbol{Q})||\boldsymbol{\eta}||^2 \tag{A-3}$$

where $\lambda_m(\cdot)$ and $\lambda_M(\cdot)$ indicate the minimum and the maximum eigenvalue. Assuming $|\dot{h}|\leq M$ and taking into account (A-2) and (A-3), the following inequality can be obtained from (A-1):

$$\dot{V}(\boldsymbol{\eta})\leq-\frac{\lambda_m(\boldsymbol{Q})}{\epsilon}||\boldsymbol{\eta}||^2+\beta||\boldsymbol{\eta}|| \tag{A-4}$$

where $\beta=2M||\boldsymbol{P}\boldsymbol{b}||$.

Now, considering (A-2), we can write

$$\dot{V}(\boldsymbol{\eta})\leq-\frac{\lambda_m(\boldsymbol{Q})}{\epsilon\lambda_M(\boldsymbol{P})}V(\boldsymbol{\eta})+\frac{\beta}{\sqrt{\lambda_m(\boldsymbol{P})}}\sqrt{V(\boldsymbol{\eta})}. \tag{A-5}$$

Since $\frac{d}{dt}\sqrt{V(\boldsymbol{\eta})}=\frac{\dot{V}(\boldsymbol{\eta})}{2\sqrt{V(\boldsymbol{\eta})}}$, we have

$$\frac{d}{dt}\sqrt{V(\boldsymbol{\eta})}\leq-\frac{\lambda_m(\boldsymbol{Q})}{2\epsilon\lambda_M(\boldsymbol{P})}\sqrt{V(\boldsymbol{\eta})}+\frac{\beta}{2\sqrt{\lambda_m(\boldsymbol{P})}} \tag{A-6}$$

which is a differential inequality, whose solution, according to [29], is

$$\sqrt{V(\boldsymbol{\eta})}\leq\left(\sqrt{V(\boldsymbol{\eta}(0))}-\frac{\epsilon\beta\lambda_M(\boldsymbol{P})}{\sqrt{\lambda_m(\boldsymbol{P})}\lambda_m(\boldsymbol{Q})}\right)e^{-\frac{\lambda_m(\boldsymbol{Q})}{2\epsilon\lambda_M(\boldsymbol{P})}t}$$
$$+\frac{\epsilon\beta\lambda_M(\boldsymbol{P})}{\sqrt{\lambda_m(\boldsymbol{P})}\lambda_m(\boldsymbol{Q})}. \tag{A-7}$$

Equation (A-7) shows that

$$\forall\gamma>0,\exists\bar{t}(\gamma):\sqrt{V(\boldsymbol{\eta})}-\frac{\epsilon\beta\lambda_M(\boldsymbol{P})}{\sqrt{\lambda_m(\boldsymbol{P})}\lambda_m(\boldsymbol{Q})}\leq\gamma\ \forall t\geq\bar{t},(\gamma) \tag{A-8}$$

which implies that

$$||\boldsymbol{\eta}||-\frac{\epsilon\beta\lambda_M(\boldsymbol{P})}{\lambda_m(\boldsymbol{P})\lambda_m(\boldsymbol{Q})}\leq\frac{\gamma}{\sqrt{\lambda_m(\boldsymbol{P})}}\qquad\forall t\geq\bar{t}(\gamma). \tag{A-9}$$

It follows that

$$||\boldsymbol{\eta}||\leq\nu=\frac{\epsilon\beta\lambda_M(\boldsymbol{P})}{\lambda_m(\boldsymbol{P})\lambda_m(\boldsymbol{Q})}+\frac{\gamma}{\sqrt{\lambda_m(\boldsymbol{P})}}\qquad\forall t\geq\bar{t}(\gamma). \tag{A-10}$$

As to be proven. ■

Remark 7: It is useful to highlight that (A-7) shows that for $t=0$, we have $\sqrt{V(\boldsymbol{\eta})}=\sqrt{V(\boldsymbol{\eta}(0))}$, whereas at the increasing of t, $\sqrt{V(\boldsymbol{\eta})}$ is bounded from

$$\sqrt{V(\boldsymbol{\eta})}\leq\sqrt{V(\boldsymbol{\eta}(0))}+\frac{\epsilon\beta\lambda_M(\boldsymbol{P})}{\sqrt{\lambda_m(\boldsymbol{P})}\lambda_m(\boldsymbol{Q})} \tag{A-11}$$

in the worst case. Moreover, (A-7) shows that for $t\to\infty$, $\sqrt{V(\boldsymbol{\eta})}$ converges within a ball whose radius is $\frac{\epsilon\beta\lambda_M(\boldsymbol{P})}{\sqrt{\lambda_m(\boldsymbol{P})}\lambda_m(\boldsymbol{Q})}$ and, consequently, $\|\eta\|$ is always bounded during transient and converges asymptotically within a ball centered at the origin, with radius given in (A-9). So it can be concluded that the error is bounded from an exponential function also during transient, and this bound depends from ϵ, which is a design parameter, and from the eigenvalues of matrices $\boldsymbol{P}$ and $\boldsymbol{Q}$. ⌟

REFERENCES

[1] P. Vas, *Sensorless Vector and Direct Torque Control*. Oxford, U.K.: Oxford Univ. Press, 1998.

[2] A. De Luca and G. Ulivi, "Design of an exact nonlinear controller for induction motors," *IEEE Trans. Autom. Control*, vol. 34, no. 12, pp. 1304–1307, Dec. 1989.

[3] D.-I. Kim, I.-J. HA, and M.-S. KO, "Control of induction motors via feedback linearization with input-output decoupling," *Int. J. Control*, vol. 51, no. 4, pp. 863–883, 1990.

[4] R. Marino, P. Tomei, and C. M. Verrelli, *Induction Motor Control Design*. New York, NY, USA: Springer-Verlag, 2010.

[5] A. Accetta, F. Alonge, M. Cirrincione, M. Pucci, and A. Sferlazza, "Feedback linearizing control of induction motor considering magnetic saturation effects," *IEEE Trans. Ind. Appl.*, vol. 52, no. 6, pp. 4843–4854, Nov./Dec. 2016.

[6] F. Alonge, M. Cirrincione, M. Pucci, and A. Sferlazza, "Input-output feedback linearizing control of linear induction motor taking into consideration the end-effects. Part I: Theoretical analysis," *Control Eng. Pract.*, vol. 36, pp. 133–141, 2015.

[7] R. Marino, S. Peresada, and P. Valigi, "Adaptive input-output linearizing control of induction motors," *IEEE Trans. Autom. Control*, vol. 38, no. 2, pp. 208–221, Feb. 1993.

[8] F. Alonge, M. Cirrincione, M. Pucci, and A. Sferlazza, "Input-output feedback linearization control with on-line MRAS based inductor resistance estimation of linear induction motors including the dynamic end-effects," *IEEE Trans. Ind. Appl.*, vol. 52, no. 1, pp. 254–266, Jan./Feb. 2016.

[9] F. Alonge, M. Cirrincione, F. D'Ippolito, M. Pucci, and A. Sferlazza, "Adaptive feedback linearizing control of linear induction motor considering the end-effects," *Control Eng. Pract.*, vol. 55, pp. 116–126, 2016.

[10] Z. Gao, Y. Huang, and J. Han, "An alternative paradigm for control system design," in *Proc. 40th IEEE Conf. Decision Control*, 2001, vol. 5, pp. 4578–4585.

[11] J. Han, "From PID to active disturbance rejection control," *IEEE Trans. Ind. Electron.*, vol. 56, no. 3, pp. 900–906, Mar. 2009.

[12] Y. Huang and W. Xue, "Active disturbance rejection control: Methodology and theoretical analysis," *ISA Trans.*, vol. 53, no. 4, pp. 963–976, 2014.
[13] B.-Z. Guo and Z.-l. Zhao, "On the convergence of an extended state observer for nonlinear systems with uncertainty," *Syst. Control Lett.*, vol. 60, no. 6, pp. 420–430, 2011.
[14] B. Du, S. Wu, S. Han, and S. Cui, "Application of linear active disturbance rejection controller for sensorless control of internal permanent magnet synchronous motor," *IEEE Trans. Ind. Electron.*, vol. 63, no. 5, pp. 3019–3027, May 2016.
[15] J. Yao, Z. Jiao, and D. Ma, "Adaptive robust control of DC motors with extended state observer," *IEEE Trans. Ind. Electron.*, vol. 61, no. 7, pp. 3630–3637, Jul. 2014.
[16] S. Zheng, B. Han, and L. Guo, "Composite hierarchical antidisturbance control for magnetic bearing system subject to multiple external disturbances," *IEEE Trans. Ind. Electron.*, vol. 61, no. 12, pp. 7004–7012, Dec. 2014.
[17] X. Chang, Y. Li, W. Zhang, N. Wang, and W. Xue, "Active disturbance rejection control for a flywheel energy storage system," *IEEE Trans. Ind. Electron.*, vol. 62, no. 2, pp. 991–1001, Feb. 2015.
[18] H. Sira-Ramírez, C. López-Uribe, and M. Velasco-Villa, "Linear observer-based active disturbance rejection control of the omnidirectional mobile robot," *Asian J. Control*, vol. 15, no. 1, pp. 51–63, 2013.
[19] M. Ramírez-Neria, H. Sira-Ramírez, R. Garrido-Moctezuma, and A. Luviano-Juarez, "Linear active disturbance rejection control of underactuated systems: The case of the Furuta pendulum," *ISA Trans.*, vol. 53, no. 4, pp. 920–928, 2014.
[20] S. Zhao and Z. Gao, "An active disturbance rejection based approach to vibration suppression in two-inertia systems," *Asian J. Control*, vol. 15, no. 2, pp. 350–362, 2013.
[21] H. Tang and Y. Li, "Development and active disturbance rejection control of a compliant micro-/nanopositioning piezostage with dual mode," *IEEE Trans. Ind. Electron.*, vol. 61, no. 3, pp. 1475–1492, Mar. 2014.
[22] J. Li, H.-P. Ren, and Y.-R. Zhong, "Robust speed control of induction motor drives using first-order auto-disturbance rejection controllers," *IEEE Trans. Ind. Appl.*, vol. 51, no. 1, pp. 712–720, Jan./Feb. 2015.
[23] L. Liu, Y. Zhang, and Q. Yao, "Induction motor drive system based on linear active disturbance rejection controller," in *Proc. Int. Conf. Mech. Eng. Control Syst.*, 2015, pp. 267–271.
[24] G. Feng, Y.-F. Liu, and L. Huang, "A new robust algorithm to improve the dynamic performance on the speed control of induction motor drive," *IEEE Trans. Power Electron.*, vol. 19, no. 6, pp. 1614–1627, Nov. 2004.
[25] H. Sira-Ramirez, F. Gonzalez-Montanez, J. A. Cortés-Romero, and A. Luviano-Juárez, "A robust linear field-oriented voltage control for the induction motor: experimental results," *IEEE Trans. Ind. Electron.*, vol. 60, no. 8, pp. 3025–3033, Aug. 2013.
[26] J.-J. E. Slotine and W. Li, *Applied Nonlinear Control*, vol. 199, no. 1. Englewood Cliffs, NJ, USA: Prentice-Hall, 1991.
[27] Q. Zheng, L. Gao, and Z. Gao, "On stability analysis of active disturbance rejection control for nonlinear time-varying plants with unknown dynamics," in *Proc. IEEE Conf. Decision Control*, New Orleans, LA, USA, Dec. 2007, pp. 12–14.
[28] A. Sferlazza and L. Zaccarian, "Linear flux observers for induction motors with quadratic Lyapunov certificates," in *Proc. IEEE 25th Int. Symp. Ind. Electron.*, 2016, pp. 167–172.
[29] N. Lungu and D . Popa, "On some differential inequalities," in *Proc. Seminar Fixed Point Theory*, 2002, vol. 3, pp. 323–327.

Francesco Alonge (M'02) was born in Agrigento, Italy, in 1946. He received the Laurea degree in electronic engineering from the University of Palermo, Palermo, Italy, in 1972.

Since then, he has been with the University of Palermo, where he is currently a Full Professor of automatic control in the Department of Systems and Control Engineering. His research topics include electrical drive control (including linear and nonlinear observers, stochastic observers, and parametric identification), robot control, parametric identification and control in power electronics, and UAV motion control in aeronautics.

Maurizio Cirrincione (M'03–SM'10) received the Laurea degree in electrical engineering from the Polytechnic University of Turin, Turin, Italy, in 1991, and the Ph.D. degree in electrical engineering from the University of Palermo, Palermo, Italy, in 1996.

Since 1996, he has been a Researcher with the Institute on Intelligent Systems for Automation—Italian National Research Council, Section of Palermo, Palermo, Italy. Since September 2005, he has been a Professor at the Université de Technologie de Belfort-Montbéliard, Belfort, France. Since April 2014, he has been the Head of the School of Engineering and Physics, University of the South Pacific, Suva, Fiji Islands. He is an author of more than 150 papers, 55 of which were published in high impact factor journals, and of two books. His current research interests include neural networks for modeling and control, system identification, intelligent control, power electronics, power quality, renewable energy systems, and electrical machines and drives.

Dr. Cirrincione received the 1997 "E. R. Caianiello" Prize for the Best Italian Ph.D. thesis on neural networks.

Filippo D'Ippolito (M'00) was born in Palermo, Italy, in 1966. He received the Laurea degree in electronic engineering in 1991 and the Research Doctorate degree in systems and control engineering in 1996, both from the University of Palermo, Palermo.

He is currently a Research Associate in the Department of Systems and Control Engineering at the University of Palermo. His research interests include control of electrical drives, control of electrical power converters, adaptive and visual/force control of robot manipulators, rehabilitation robotics, and marine robotics.

Dr. D'Ippolito received the 2000 Kelvin Premium from the Institution of Electrical Engineers, U.K., for the paper "Parameter identification of induction motor model using genetic algorithms."

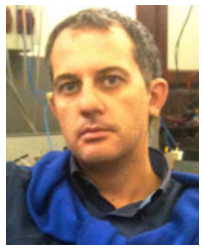

Marcello Pucci (M'03–SM'11) received the Laurea and Ph.D. degrees in electrical engineering from the University of Palermo, Palermo, Italy, in 1997 and 2002, respectively.

In 2000, he was a Host Student with the Institute of Automatic Control, Technical University of Braunschweig, Braunschweig, Germany, working in the field of control of ac machines, with a grant from the German Academic Exchange Service. Since 2001, he has been with the Institute of Intelligent Systems for Automation, Section of Palermo, National Research Council of Italy, Palermo, where he is currently a Senior Researcher. His current research interests include electrical machines; control, diagnosis, and identification techniques of electrical drives; and intelligent control and power converters.

Dr. Pucci is an Associate Editor of the IEEE TRANSACTIONS ON INDUSTRIAL ELECTRONICS and the IEEE TRANSACTIONS ON INDUSTRY APPLICATIONS. He is a member of the Editorial Board of the *Journal of Electrical Systems*.

Antonino Sferlazza (S'12–M'15) was born in Palermo, Italy, in November 1987. He received the Master's degree in automation engineering and the Ph.D. degree in mathematics and automation from the University of Palermo, Palermo, in 2011 and 2015, respectively.

He is currently a Research Fellow in systems and control engineering in the Department of Energy, Information Engineering, and Mathematical Models, University of Palermo. His research interests include the development of feedback control algorithms for nonlinear dynamical systems, optimization techniques, estimation of stochastic dynamical systems, and applications of control of electrical drives, power converters, and mechanical systems.